Medical Oncology (2025) 42:242
https://doi.org/10.1007/s12032-025-02794-2

ORIGINAL PAPER

CEBPB regulates ERK1/2 activity through SOS1 and contributes to ovarian cancer progression

Jiahong Tan[1] · Daoqi Wang[2] · Aiqing Tu[1] · Qin Xu[1] · Li Zhuan[1] · Xiaodie Wu[1] · Lin Zhao[1] · Wei Dong[1] · Jie Zhang[1] · Yun Feng[1]

Received: 18 March 2025 / Accepted: 15 May 2025

Abstract

Ovarian cancer (OC) is among the most prevalent malignant tumors affecting the female reproductive system. Notably, CEBPB has emerged as a highly promising biomarker, attracting substantial attention for its role in mediating chemotherapy resistance to PARP inhibitors (PARPi). However, the precise mechanism of action of CEBPB in OC remains poorly understood. CCK-8 assays, colony formation assays, transwell assays, and wound healing assays were employed to assess malignant behaviors of OC cells. Flow cytometry was utilized to analyze cell apoptosis and cell cycle progression. qRT-PCR and Western blot analyses were performed to quantify the levels of SOS1 and phosphorylated ERK1/2 (p-ERK1/2). Overexpression of CEBPB enhanced the proliferation, colony formation ability, invasion, migration, and cell cycle progression of SKOV3 and A2780 OC cells, while simultaneously inhibiting their apoptosis. Conversely, knockdown of CEBPB produced opposite effects ($p < 0.01$). Results from the MAPK Signaling Pathway PCR Array and Western blot analyses indicated that CEBPB increases the expression of SOS1 ($p < 0.01$). Additionally, dual-luciferase reporter assays demonstrated that CEBPB binds to the promoter sequence of the target gene SOS1. CEBPB knockdown significantly inhibited the malignant behavior of OC cells and reduced the levels of p-ERK1/2, whereas overexpression of SOS1 partially reversed this effect ($p < 0.01$). In xenograft models, CEBPB activates ERK1/2 via SOS1 upregulation, which subsequently promotes tumor growth and suppresses apoptosis ($p < 0.01$). CEBPB regulates ERK1/2 activity through SOS1 and contributes to OC progression.

Keywords Ovarian cancer · CEBPB · SOS1 · ERK1/2

Abbreviations

FBS	Fetal bovine serum
GEF	Guanine nucleotide exchange factor
HE	Hematoxylin–eosin
IHC	Immunohistochemistry
OC	Ovarian cancer
PARPi	PARP inhibitors
PDXs	Patient-derived xenografts
PI	Proliferation index
RT	Room temperature
SOS	Son of sevenless

Introduction

Ovarian cancer (OC), one of the most prevalent malignant tumors affecting the female reproductive system, ranks third in morbidity and exhibiting the highest mortality rate [1]. Approximately 90% of ovarian cancers arise from the tumorigenic transformation of normal ovarian epithelial cells, a process known as epithelial OC [2]. In 2024, the United States anticipates an estimated 2,001,140 new cancer cases and 611,720 cancer-related deaths, with OC accounting for 19,680 new diagnoses and 12,740 deaths. This demonstrates a particularly high mortality burden, as evidenced by an overall 5-year survival rate of just 49% [3, 4]. Early-stage OC often lacks specific symptoms, typically presenting with

✉ Daoqi Wang
daoqi_w@163.com; daoqi_w@outlook.com

✉ Wei Dong
weiwei_d@126.com

[1] Department of Obstetrics and Gynecology, The First People's Hospital of Yunnan Province, The Affiliated Hospital of Kunming University of Science and Technology, No.157 Jinbi Road, Kunming 650032, People's Republic of China

[2] Department of Urology, The Second Affiliated Hospital of Kunming Medical University, No.374 Dianmian Avenue, Kunming 650101, People's Republic of China

Published online: 07 June 2025

nonspecific complaints such as abdominal or pelvic pain, bloating, difficulty eating, and urinary issues. Consequently, it is frequently misdiagnosed initially and is usually identified only after metastasis has occurred [5]. Currently, useful serum tumor markers that aid in the clinical diagnosis of OC include CA125, HE4, CEA, AFP, and CA199, among others [6]. Although these markers are widely used, their individual diagnostic value remains limited. Therefore, the joint detection of multiple indicators has emerged as a promising trend in the early diagnosis of clinical OC. The introduction of PARP inhibitors (PARPi) has revolutionized the treatment landscape for OC. Evidence shows that PARPi are highly effective both as initial treatment and for platinum-sensitive recurrent OC. While PARPi maintenance therapy following response can significantly extend progression-free survival, its impact on overall survival remains limited [7]. In conclusion, the challenges of early diagnosis and chemotherapy resistance contribute to OC's poor prognosis. Further research into OC pathogenesis and the identification of molecular biomarkers are essential for improving outcomes.

CEBPB, a member of the leucine zipper transcription factor family, plays significant roles in various biological processes, including cell proliferation, differentiation, apoptosis, oncogene-induced senescence, and tumor development [8–11]. Currently, the regulation of target genes by CEBPB in OC remains underexplored. Existing studies indicate that LINC00035 promotes OC progression by influencing glycolysis and apoptosis through the CEBPB-mediated transcription of SLC16A3 [12]. Additionally, COL11A1 has been shown to induce chemotherapy resistance in OC cells, with a CEBPB binding site in the COL11A1 promoter serving as the primary determinant of COL11A1 activation by anticancer drugs [13]. Furthermore, PARPi have demonstrated high efficacy in treating high-grade serous OC characterized by homologous recombination deficiency [14]. Studies have identified CEBPB as a key regulator of the homologous recombination pathway, as it directly targets and upregulates several homologous recombination genes, thereby restoring homologous recombination capability and mediating acquired resistance to PARPi [8, 15, 16]. Consequently, CEBPB may serve as a potential indicator of PARPi response. Given the critical role of PARPi in OC treatment, further investigation into the functional mechanisms of CEBPB in this context is warranted.

The guanine nucleotide exchange factor Son of Sevenless (SOS) family comprises two members: SOS1 and SOS2 [17]. Under upstream signaling, SOS1 is recruited to the cell membrane via Grb2 binding, where it acts as a guanine nucleotide exchange factor (GEF) for RAS, promoting RAS activation [18]. Studies have shown that mutated K-RAS activates wild-type RAS (H-RAS and N-RAS) through SOS1-mediated allostery, and this activated wild-type RAS drives tumor progression via the ERK/MAPK/JNK pathway [19]. Therefore, SOS1 is a key regulator of ERK1/2 activation. Moreover, CEBPB undergoes phosphorylation via the RAS/MAPK pathway [20, 21], and its transcriptional activation potential is stimulated by either Ca2 + /calmodulin-dependent protein kinase or ERK1/2 [22, 23]. Collectively, these findings establish that CEBPB and SOS1 as pivotal regulators of the RAS/MAPK/ERK/JNK cascade. Therefore, we investigated the mechanism through which CEBPB regulates ERK1/2 activity via SOS1, thereby promoting OC progression. Our study elucidates this mechanism using both in vitro and in vivo models, providing theoretical foundation for OC treatment.

Materials and methods

Cells and animal sources

Human OC cell lines SKOV3 and A2780 were obtained from the Henan Industrial Microbial Culture Engineering Technology Research Center. Twenty-four 6-week-old, SPF-grade female BALB/c nude mice, weighing 18–22 g were purchased from Beijing Vital River Laboratory Animal Technology Co. (Animal certification number: 1017820638302109831). The mice were housed under controlled conditions: temperature maintained at (25 ± 1)℃, humidity at 40%-60%, and a 12 h light/dark cycle. All experiments complied with ARRIVE guidelines and were approved by the Institutional Animal Care and Use Committee (IACUC) of Kunming Medical University (approval number: KMMU20241878).

Cell culture and experimental groups

SKOV3 and A2780 cells were cultured in RPMI-1640 medium supplemented with 10% fetal bovine serum (FBS) at 37 ℃ under 5% CO_2 in a humidified cell culture incubator. Cells were harvested at the logarithmic growth phase (~ 80% confluency) and systematically allocated into the following five experimental groups: blank control (BC), negative control (NC), CEBPB knockdown (sh-CEBPB), CEBPB overexpression (OE-CEBPB), and CEBPB knockdown combined with SOS1 overexpression (sh-CEBPB + OE-SOS1). Short hairpin RNAs (shRNAs) targeting CEBPB, along with OE-CEBPB and OE-SOS1 lentivirus vectors, were obtained from Tsingke Biotechnology Co., Ltd. Cells were subsequently infected with sh-CEBPB, OE-CEBPB, and OE-SOS1 lentiviral vectors, and their corresponding empty lentiviral vectors. The shRNA sequences used for CEBPB knockdown were as follows: sh-CEBPB 1#: 5′-GCACAG CGACGAGTACAAGAT-3′, sh-CEBPB 2#: 5′-CCTGCG GAACTTGTTCAAGCA-3′, sh-CEBPB 3#: 5′-CAACCT GGAGACGCAGCACAA-3′, and sh-CEBPB 4#: 5′-GCT

GCGCGCTTACCTCGGCTA-3′. After 48 h of transfection, the transfection efficiency was assessed via qRT-PCR [24].

qRT-PCR

Total RNA was extracted from each experimental group, and qPCR was performed according to the manufacturer's protocols using Tiangen Biochemical Technology Co.'s reverse transcription and SYBR Green PCR kits. The PCR reaction parameters included 95 ℃ for 30 s, followed by 95 ℃ for 10 s, and 65 ℃ for 30 s, for a total of 40 cycles. The relative expression of target genes was quantified using the 2-ΔΔCt method with GAPDH as the internal reference gene. The primer sequences were as follows: CEBPB (F: 5′-TTTGTCCAAACCAACCGCAC-3′, R: 5′-GCATCAACT TCGAAACCGGC-3′), SOS1 (F: 5′-CGAGCCCTTTTCACT CAAGC-3′, R: 5′-GCCATGGGGCAGAGTAACTT-3′), and GAPDH (F: 5′-AGACCACAGTCCATGCCATC-3′, R: 5′-CAGGGCCCTTTTTCTGAGCC-3′).

CCK-8 assay

As previously described [25], cell proliferation was evaluated using the CCK-8 assay (Cat#C0039, Beyotime). After cell counting, cells were seeded into 96-well plates. Using the cell attachment time point as 0 h, 10 μL of CCK-8 solution was added to each well containing 90 μL of serum-free medium at specified time points, followed by 1 h incubation. Absorbance was measured at 450 nm using a microplate reader.

MAPK signaling pathway PCR array

Total RNA was extracted using TRIzol reagent. Following quality control by UV absorption and agarose gel electrophoresis, cDNA was synthesized and subsequently used for qRT-PCR to evaluate expression of MAPK signaling pathway genes and identify differentially expressed genes. The MAPK Signaling Pathway PCR Array was purchased from Shanghai Woji Gene Technology Co. Ltd.

Colony formation assay

A total of 3000 cells per well were seeded in 12-well plates and incubated for14 days. The cells were fixed with 4% paraformaldehyde for 4 h and stained with 1% crystal violet for 5 min. After PBS washing, the cells were counted under a microscope in five randomly chosen fields, and images were captured.

Transwell assay

Cells (1 × 10^5 per chamber) were seeded in serum-free medium in the upper chamber, while the lower chamber contained medium supplemented with 15% FBS. After 48 h of incubation, cells that migrated to the lower chamber were fixed with 4% paraformaldehyde for 4 h, stained with 1% crystal violet for 5 min, and washed with PBS. The stained cells were then examined and quantified under a microscope.

Cell scratch healing experiment

As previously described [26], cell migration was evaluated using a wound healing assay. Cells were seeded in 6-well plates (2 × 10^6 cells/well), and horizontal reference lines were marked on the plate bottom at 0.5–1 cm intervals. At ~ 80% confluence after 20 h, a straight scratch was generated using a pipette tip held vertically. The wells were washed twice with serum-free medium to remove debris, replenished with fresh serum-free medium, and cultured at 37 ℃ with 5% CO2. Images of identical fields were captured at 0 and 24 h.

Flow cytometry detection of apoptosis

Cells were seeded in 6-well plates and cultured overnight. Both apoptotic cells and detached adherent cells in the supernatant were collected. Cell pellets were washed with ice-cold PBS, then resuspended in 100 μL binding buffer. Subsequently, 5 μL Annexin V-FITC (Cat#C1062L, Beyotime) and 5 μL propidium iodide (PI) were added, followed by a 15 min incubation at 4 °C in the dark. Finally, cells were analyzed by flow cytometry.

Flow cytometry analysis of cell cycle distribution

Cells from each group were collected, washed twice with PBS, and fixed in 70% ethanol overnight at 4 °C. The fixed cells were then washed twice with PBS, resuspended in 100 μL RNAse A solution, and incubated at 37 °C for 30 min. Next, 100 μL PI solution was added and mixed thoroughly. After an additional 30 min incubation, samples were analyzed by flow cytometer with 488 nm excitation. The proliferation index (PI) was calculated as: PI = (S + G2/M) / (G0/G1 + S + G2/M).

Dual-luciferase reporter experiment

The wild-type (WT) and mutant type (MUT) SOS1 3′ UTR luciferase reporter vectors were constructed and designated as SOS1-WT and SOS1-MUT, respectively. These luciferase plasmids synthesized by Beijing Tsingke Biotechnology Co., Ltd. Cells were seeded in 24-well plates and divided

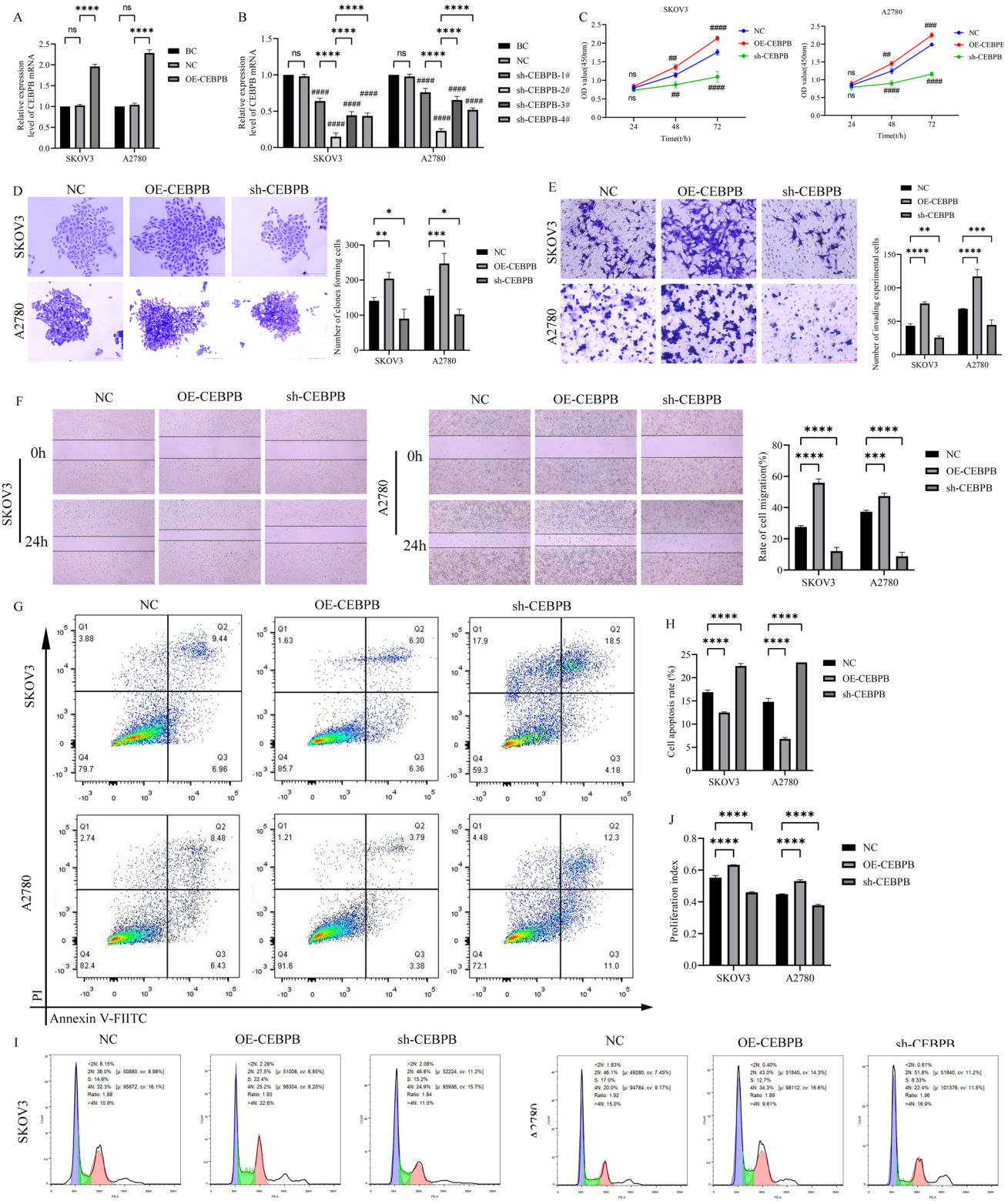

into five experimental groups: NC, SOS1-WT + OE-NC, SOS1-WT + OE-CEBPB, SOS1-MUT + OE-NC, and SOS1-MUT + OE-CEBPB, with three replicate wells for each group. After 48 h of transfection using Lipofectamine™ 2000, dual-luciferase activity was measured with the Dual-Luciferase® Reporter Assay System (Promega).

◂**Fig. 1** CEBPB promotes malignant behavior of OC cells. **A**, **B** the overexpression and knockdown efficiency of CEBPB was detected by qRT-PCR (# represents $p < 0.05$ in the comparison with the NC group); **C** the proliferation ability of SKOV3 and A2780 cells was detected by CCK-8 kit (# represents $p < 0.05$ in the comparison with the NC group); **D** the colony formation ability of cells was detected by colony formation assay and its statistical graph (scale bar = 50 μm); **E** cell invasion ability was detected by Transwell assay and its statistical graph (scale bar = 50 μm); **F** cell migration ability was detected by scratch healing assay and its statistical graph (scale bar = 50 μm); **G**, **H** cell apoptosis rate was detected by flow cytometry and its statistical graph; **I**, **J** cell cycle changes were assessed by flow cytometry and its statistical graph. Plots are representative of three independent replicate experiments ($n = 3$ per group per experiment). *, $p < 0.05$; **, $p < 0.01$; ***, $p < 0.001$; ****, $p < 0.0001$; ns, not statistically significant

Tumorigenesis experiments in nude mice

A2780 cell suspension was subcutaneously injected into nude mice at 1 × 10^7 cells/mL. Mice were divided into three groups: a negative control (NC) group, a CEBPB overexpression group (OE-CEBPB), where A2780 cells with CEBPB overexpression were injected, and a CEBPB knockdown group (sh-CEBPB), where A2780 cells with CEBPB knockdown were injected. Each group consisted of 8 mice. Tumor dimensions were measured every 3 days from day 0 to 27 post-injection using a vernier caliper: long diameter (a) and short diameter (b). Tumor volume was calculated as $0.5 \times a \times b^2$. Growth curves were plotted until tumors reached ~ 1000 mm^3. At 4 weeks, mice were euthanized via intraperitoneal injection of pentobarbital sodium (100 mg/kg). Death was confirmed by cessation of breathing, absent heartbeat, and fixed pupil dilation. Tumors were excised and weighed on day 28.

Hematoxylin–eosin (HE) staining

After 24 h of fixation, tumor tissues were processed through paraffin embedding, sectioned, and mounted. Sections were deparaffinized in xylene, rehydrated through an ethanol gradient, stained with Harris' hematoxylin and 0.5% eosin, dehydrated through another ethanol gradient, and coverslipped. Finally, sections were imaged under a microscope.

TUNEL staining

Frozen sections were air-dried at room temperature (RT) for 30 min, washed twice with PBS (5 min per wash), and permeabilized in PBS containing 0.3% Triton X-100 for 5 min at RT. Sections were then incubated with TUNEL assay solution (#C1091, Beyotime) for 1 h at 37 ℃ in the dark, followed by three 5 min PBS washes. Nuclei were counterstained with DAPI (1 μg/mL) for 20 min at RT in the dark, washed thrice with PBS (5 min each), and mounted with antifade medium. TUNEL-positive cells were quantified using ImageJ from fluorescence micrographs.

Western blot

Cells or tissues were ground and homogenized using RIPA lysis buffer to extract total protein. Protein concentrations were determined by BCA assay. SDS-PAGE gels (10% or 15%) were prepared based on target protein molecular weights. After heat-denaturation at 100 ℃ for 10 min, equal protein amounts were loaded for electrophoresis. Separated proteins were transferred to PVDF membranes, blocked with 5% skim milk in TBST for 2 h at RT, and incubated overnight at 4 ℃ with primary antibodies: SOS1 (Cat#ab140621, Abcam), CEBPB (Cat#43095, CST), p-ERK1/2 (Cat#ab278538, Abcam), and β-actin (Cat#AF5003, Beyotime). After TBST washes, membranes were incubated for 2 h at RT with HRP-conjugated goat anti-rabbit IgG(H + L) (#A0208, Beyotime). Signals were detected by ECL using a chemiluminescence imager, and band intensities were quantified with ImageJ.

Tissue immunofluorescence staining

Tumor tissues were fixed in 4% paraformaldehyde, dehydrated through a graded sucrose series (20% and 30%), embedded in OCT compound, and sectioned at 5 μm thickness. Sections were immunostained with: Rabbit anti-CEBPB monoclonal antibody (Cat#43095, CST) or rabbit anti-SOS1 monoclonal antibody (Cat#ab140621, Abcam). After overnight incubation at 4 ℃ and 1 h rewarming at RT, sections were PBS-washed and incubated with Alexa Fluor 350-conjugated goat anti-rabbit IgG(H + L) (#A0408, Beyotime) in a humidified chamber for 2 h in the dark. Following PBS washes, nuclei were counterstained with DAPI for 15 min in a light-protected humid chamber, then washed again. Sections were mounted with antifade medium and imaged using a confocal microscope. Fluorescence intensity was quantified using ImageJ.

Immunohistochemistry (IHC)

Tissue specimens were fixed in 4% paraformaldehyde, paraffin-embedded, and sectioned at 4 μm. After xylene deparaffinization, sections were rehydrated through an ethanol gradient (100%, 95%, 85%, 75%), treated with 3% H_2O_2 for 10 min to block endogenous peroxidases, and subjected to heat-mediated antigen retrieval for 2 min. Following three 3-min PBS washes, sections were incubated with peroxidase blocking reagent for 15 min at RT. Primary antibody incubation used rabbit anti-Ki67 (#AF1738, Beyotime) overnight

at 4 ℃. After PBS washes, nonspecific binding was blocked with 50 µL normal serum for 20 min. Sections were then incubated with HRP-conjugated goat anti-rabbit IgG(H + L) (#A0208, Beyotime) for 30 min at RT, followed by three PBS washes. Chromogenic development used DAB substrate with hematoxylin counterstaining. Sections were dehydrated through a reverse ethanol series, cleared in xylene, mounted with resin, and imaged by bright-field microscopy.

Statistical analysis

Image analysis was performed using ImageJ, while statistical analyses were conducted with GraphPad Prism 8.0. Data from three independent biological replicates were presented as mean ± SD. Comparisons between two groups of samples were conducted using an independent samples t-test, whereas comparisons among multiple groups of samples were performed using one-way analysis of variance. A p-value of less than 0.05 was considered statistically significant.

Results

CEBPB promotes malignant behavior of OC cells

To investigate CEBPB's role in OC cell malignancy, we established SKOV3 and A2780 cell lines with CEBPB overexpression and knockdown. The results are presented in Fig. 1A and B. Compared to the NC group, the mRNA levels in the OE-CEBPB group were significantly elevated, while the mRNA levels in the sh-CEBPB-1#, 2#, 3#, and 4# groups were markedly reduced. Notably, sh-CEBPB-2# (5′-CCTGCGGAACTTGTTCAAGCA-3′) exhibited the highest knockdown efficiency, and thus this sequence was utilized for subsequent experiments. These results confirmed the successful construction of CEBPB overexpression and knockdown models in SKOV3 and A2780 cells. The results from CCK-8 assays, colony formation assays, Transwell assays, and scratch assays demonstrated that CEBPB overexpression significantly enhanced the proliferation, colony formation ability, invasion, and migration of OC cells, whereas CEBPB knockdown exerted the opposite effects (Fig. 1C–F). Furthermore, flow cytometry analyses revealed that CEBPB overexpression significantly inhibited apoptosis and accelerated cell cycle progression in OC cells, while CEBPB knockdown had contrary effects (Fig. 1G–J). Collectively, these results demonstrate CEBPB's pivotal role in driving OC malignancy.

Regulatory effect of CEBPB expression changes on MAPK signaling pathway

To investigate CEBPB's regulatory effects on the MAPK pathway, we analyzed MAPK pathway gene expression profiles using a MAPK signaling PCR array. In SKOV3 cells, the expression levels of genes such as MAPK9, RAF1, PAK2, and SOS1 exhibited more pronounced changes following both overexpression and knockdown of CEBPB (Fig. 2A). Similarly, in A2780 cells, the expression of MAPKAPK3, MAPK9, SOS1, PKA2, and other genes showed significant alterations with CEBPB overexpression and knockdown (Fig. 2B). The MAPK chip results revealed that genes displaying consistent expression trends across both cell lines, specifically MAP4K1, PAK2, MKNK1, and SOS1, which were subsequently validated using Western blotting, as illustrated in Fig. 2C. In both SKOV3 and A2780 cells, SOS1 expression in the OE-CEBPB group was significantly elevated compared to the NC group, whereas SOS1 expression in the sh-CEBPB group was markedly downregulated. These findings suggest that CEBPB plays a regulatory role in the expression of SOS1. Therefore, SOS1 was selected for verification in subsequent experiments.

CEBPB upregulates ERK1/2 activity and promotes malignant progression of OC cells via SOS1

To investigate the mechanism by which CEBPB regulates MAPK pathway and promotes OC cell malignancy, we constructed SKOV3 and A2780 cell lines that overexpressed SOS1. qRT-PCR and Western blot analyses revealed that, compared to the NC group, both the mRNA and protein levels of SOS1 were significantly elevated in the OE-SOS1 group (Fig. 3A, B), confirming the successful establishment of SOS1-overexpressing SKOV3 and A2780 cells. Functional assays, including CCK-8, colony formation, Transwell, and scratch assays, demonstrated that CEBPB knockdown markedly inhibited the proliferation, colony formation ability, invasion, and migration of OC cells, while SOS1 overexpression partially reversed these effects (Fig. 3C–F). Flow cytometry results indicated that CEBPB knockdown significantly enhanced the apoptosis of OC cells and impeded cell cycle progression, while SOS1 overexpression partially mitigated these changes (Fig. 3G–J). To further investigate the interaction between CEBPB and SOS1, we conducted a dual-luciferase reporter assay to examine the binding of CEBPB to the promoter sequence of SOS1. The results showed that CEBPB overexpression significantly increased the luciferase activity of the WT-SOS1 group compared to the NC group, while it had no effect on the luciferase activity of

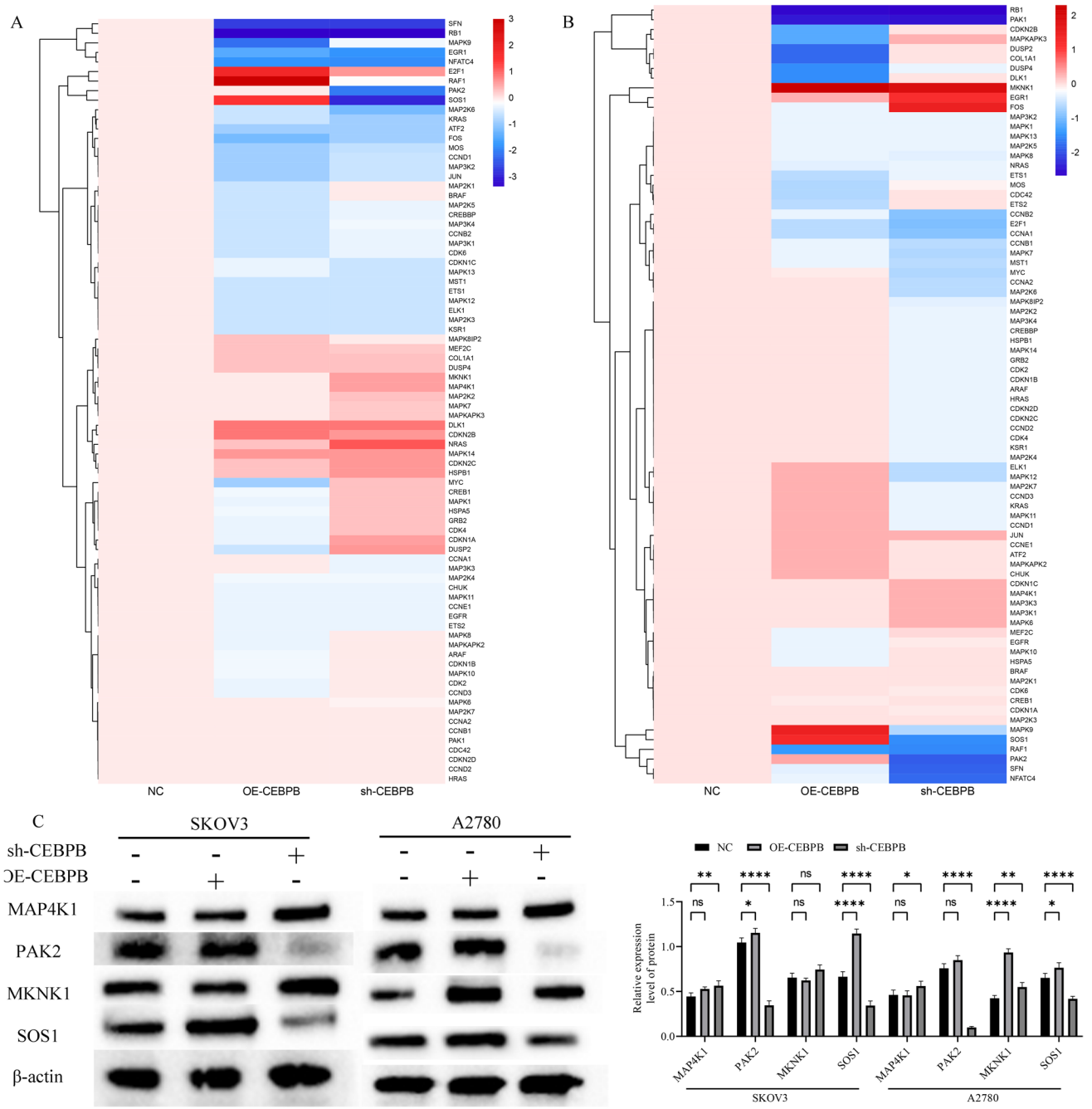

Fig. 2 The regulatory effect of changes in CEBPB expression on the MAPK signaling pathway. **A** Heatmap of genes in the MAPK pathway in SKOV3 cells; **B** Heatmap of genes in the MAPK pathway in A2780 cells; C: The expression of MAP4K1, PAK2, MKNK1 and SOS1 in SKOV3 and A2780 cells was detected by Western blotting and their statistical graphs. Plots are representative of three independent replicate experiments ($n=3$ per group per experiment). *, $p<0.05$; ***, $p<0.01$; ***, $p<0.001$; ****, $p<0.0001$; ns, not statistically significant

the MUT-SOS1 group (Fig. 3K). Additionally, qRT-PCR results demonstrated that CEBPB knockdown significantly decreased SOS1 mRNA expression, whereas SOS1 overexpression led to an increase in its mRNA levels (Fig. 3L). Western blot analysis further indicated that CEBPB knockdown significantly reduced the levels of SOS1 and phosphorylated ERK1/2, while SOS1 overexpression partially restored these levels (Fig. 3M). Collectively, these findings suggest that CEBPB upregulates SOS1, thereby promoting the malignant progression of OC cells through the ERK1/2 signaling pathway.

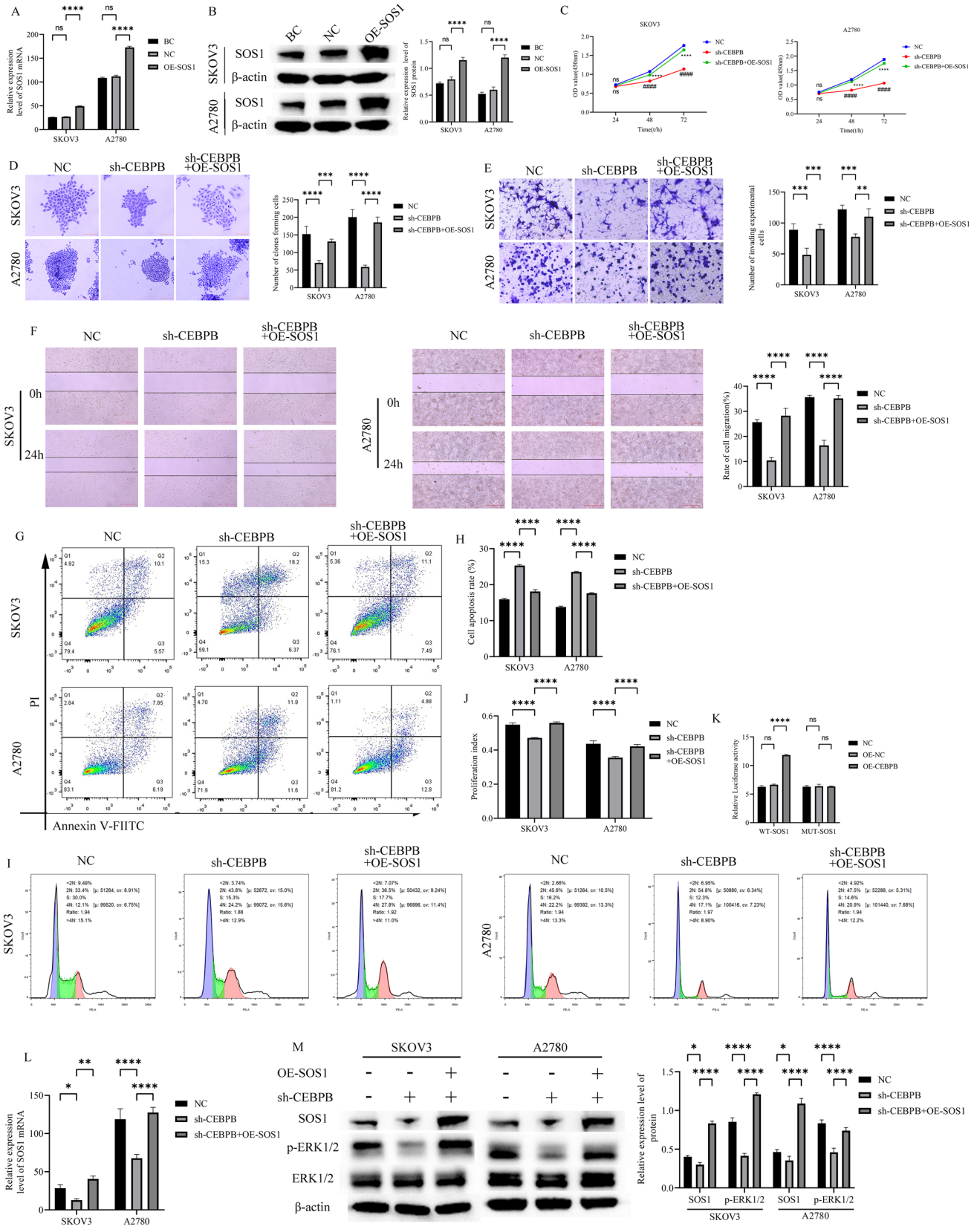
A
B
C
D
E
F
G
H
I
J
K
L
M
NC
sh-CEBPB
sh-CEBPB+OE-SOS1
BC
OE-SOS1
SKOV3
A2780
SOS1
β-actin
p-ERK1/2
ERK1/2
Relative expression level of SOS1 mRNA
Relative expression level of SOS1 protein
OD value(450nm)
Time(t/h)
Number of clones forming cells
Number of invading experimental cells
Rate of cell migration(%)
Cell apoptosis rate (%)
Proliferation index
Relative Luciferase activity
WT-SOS1
MUT-SOS1
OE-NC
OE-CEBPB
Annexin V-FITC
PI
Relative expression level of protein

◂**Fig. 3** CEBPB upregulates ERK1/2 activity to promote the malignant progression of OC cells via SOS1. **A** The expression of SOS1 mRNA in SKOV3 and A2780 cells was detected by qRT-PCR; **B** the expression of SOS1 in SKOV3 and A2780 cells was detected by Western blotting and their statistical graphs; **C** the proliferation ability of cells was detected by CCK-8 kit; **D** the colony forming ability of cells was detected by clone formation assay and its statistical graph (scale bar = 50 μm); **E** the invasion ability of cells was detected by transwell assay and its statistical graph (scale bar = 50 μm); **F** cells Migration ability was detected by scratch healing assay and its statistical graph (scale bar = 50 μm); **G**, **H** cell apoptosis rate was detected by flow cytometry and its statistical graph; **I**, **J** cell cycle changes was detected by flow cytometry and its statistical graph; **K** the binding of CEBPB to the promoter sequence of the target gene SOS1 was detected by dual-luciferase reporter experiment; **L** the expression of SOS1 mRNA was detected by qRT-PCR; **M** the levels of SOS1 and phosphorylated ERK1/2 was detected by western blotting and their statistical graphs. Plots are representative of three independent replicate experiments ($n = 3$ per group per experiment). *, $p < 0.05$; **, $p < 0.01$; ***, $p < 0.001$; ****, $p < 0.0001$; ns, not statistically significant

CEBPB upregulates ERK1/2 activity via SOS1 promoting malignant progression of OC in vivo

To investigate the mechanism by which CEBPB upregulates ERK1/2 activity via SOS1 in the malignant progression of OC, OC cells with either overexpression or knockdown of CEBPB were transfected into nude mice, establishing a subcutaneous tumor model. Once palpable tumors formed, the mice were monitored for 4 weeks, during which the volume and weight of the tumors were measured every three days. The results were depicted in Figs. 4A and B. Notably, overexpression of CEBPB significantly increased the volume of transplanted tumors in nude mice, whereas knockdown of CEBPB resulted in a significant reduction in tumor volume; however, neither overexpression nor knockdown of CEBPB had a significant impact on the body weight of the nude mice. HE staining revealed that, compared to the NC group, tumor cells in the OE-CEBPB group were more tightly packed and exhibited enlarged cells with varying morphologies and pronounced atypia. In contrast, tumor cells in the sh-CEBPB group displayed localized necrosis, along with apoptotic changes including nuclear condensation and vacuolization (Fig. 4C, upper panel). IHC results indicated that OE-CEBPB enhanced the expression of Ki67, while sh-CEBPB suppressed Ki67 expression (Fig. 4C, lower panel; Fig. 4D). Tissue immunofluorescence analysis demonstrated that OE-CEBPB significantly elevated the expression levels of CEBPB and SOS1, whereas sh-CEBPB markedly downregulated these proteins (Fig. 4E–H). TUNEL staining results indicated that OE-CEBPB inhibited apoptosis, while sh-CEBPB promoted apoptotic processes (Fig. 4I–J). Western blot analysis further confirmed that OE-CEBPB significantly increased the levels of CEBPB, SOS1, and p-ERK1/2, whereas sh-CEBPB led to a significant decrease in these protein levels (Fig. 4K–L).

Discussion

PARPi are pivotal for maintenance therapy, effectively eliminating residual tumor cells post-surgery and micrometastases undetectable during resection [27]. Their favorable safety profile and efficacy in preventing long-term recurrence have established PARPi as a guideline-recommended first-line maintenance therapy for platinum-sensitive recurrent OC [28–31]. However, acquired resistance to PARPi has emerged as a critical clinical challenge [32]. In OC, CEBPB has garnered significant attention for its role in mediating resistance to PARPi. In this study, we demonstrate for the first time that CEBPB enhances the malignant behavior of OC cells by upregulating SOS1. Furthermore, the activation of SOS1 contributes to the aggressive behavior of OC through the ERK1/2 signaling pathway. The mechanism by which CEBPB facilitates the malignant progression of OC cells by upregulating ERK1/2 activity via SOS1 was further validated in vivo.

In this study, we demonstrated that the overexpression of CEBPB enhanced the malignant behavior of OC, while its knockdown inhibited this malignancy. Additionally, dual-luciferase reporter assays confirmed that CEBPB binds to the promoter sequence of its target gene, SOS1. Importantly, knocking down CEBPB while overexpressing SOS1 partially reversed the inhibitory effects of CEBPB knockdown on the malignant behavior of OC. Previous research has shown that oncogenic RAS effectively stimulates CEBPB to activate the CEBP-responsive promoter reporter gene in keratinocytes, and mutating the ERK1/2 phosphorylation site (T188) in CEBPB abolishes this RAS effect [33]. It has been shown that CEBPB plays a key role in RAS-mediated tumorigenesis and cell survival, and evidence suggests that CEBPB is a target of tumor suppression [21]. Furthermore, selective inhibition of SOS1 significantly downregulated the levels of active RAS in tumor cells [34, 35]. In mutant tumor cell lines harboring KRAS alleles, chemical inhibition of SOS1 resulted in a 50% reduction in p-ERK activity [34]. Collectively, these studies suggest that CEBPB and SOS1 are critical proteins within the RAS signaling pathway [36]. Most importantly, this study is the first to reveal that CEBPB promotes the progression of OC through its interaction with SOS1.

The MAPK signal transduction cascade is a highly conserved central regulator of cell proliferation, cell cycle progression, and survival. It can be activated by a variety of extracellular signals, including growth factors and cytokines [37]. Currently, there are four MAPK cascades in eukaryotic cells: the ERK cascade, the p38 MAPK cascade, the JNK cascade, and the ERK5 cascade. The p38 MAPK and JNK cascades are primarily involved in the transduction of stress-related stimuli, whereas the ERK cascade is

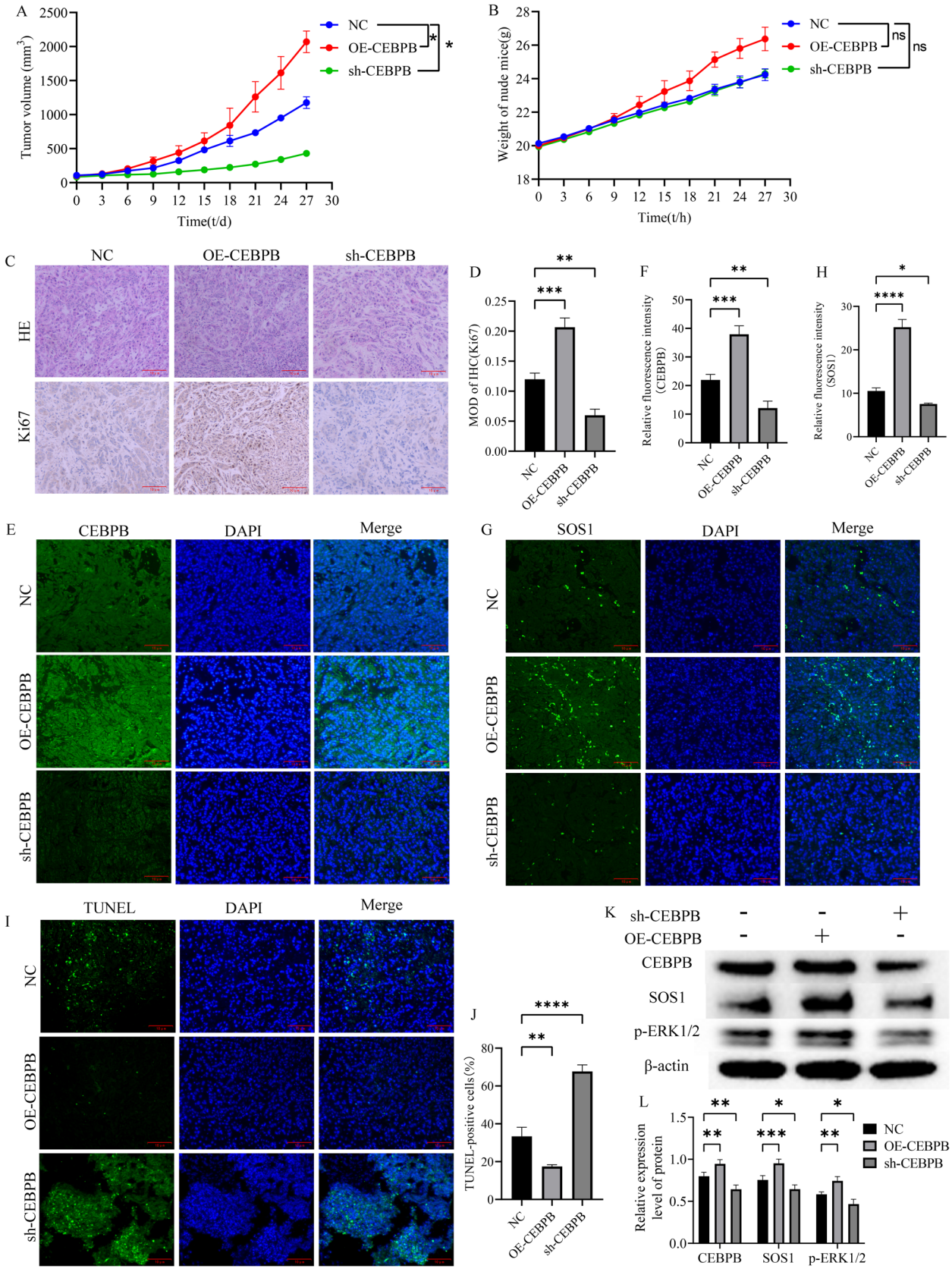
A
Tumor volume (mm3)
Time(t/d)
NC
OE-CEBPB
sh-CEBPB
B
Weight of nude mice(g)
Time(t/h)
ns
C
NC
OE-CEBPB
sh-CEBPB
HE
Ki67
D
MOD of IHC(Ki67)
F
Relative fluorescence intensity (CEBPB)
H
Relative fluorescence intensity (SOS1)
E
CEBPB
DAPI
Merge
G
SOS1
I
TUNEL
J
TUNEL-positive cells(%)
K
sh-CEBPB
OE-CEBPB
CEBPB
SOS1
p-ERK1/2
β-actin
L
Relative expression level of protein

◂**Fig. 4** CEBPB upregulates ERK1/2 activity and affects the malignant progression of OC through SOS1 in vivo. **A** Tumor volume of transplanted tumors in nude mice; **B** body weight of nude mice; **C** pathological changes of nude mice were observed by HE staining, and Ki67 expression was detected by IHC staining (scale bar = 10 μm); **D** statistical diagram of IHC results; **E**, **F** The expression of CEBPB was detected by immunofluorescence and its statistical diagram (scale bar = 10 μm); **G**, **H** The expression of SOS1 was detected by immunofluorescence and its statistical graph (scale bar = 10 μm); **I**, **J** The apoptosis of tumor tissue was detected by TUNEL staining and its statistics graph (scale bar = 10 μm); **K**, **L** the levels of CEBPB, SOS1, and phosphorylated ERK1/2 were detected by western blotting and their statistical graphs. Plots are representative of three independent replicate experiments ($n = 3$ per group per experiment). *, $p < 0.05$; **, $p < 0.01$; ***, $p < 0.001$; ****, $p < 0.0001$; ns, not statistically significant

predominantly associated with the transmission of mitotic signals, cell proliferation, migration, and differentiation [38, 39]. Among these, the ERK cascade, specifically the RAS-RAF-MEK-ERK signaling cascade, is the most extensively studied MAPK pathway and is abnormally activated in over one-third of human cancers[40, 41]. When RAS is activated by growth factors, it recruits RAF kinase to the plasma membrane for activation. Activated RAF kinase subsequently phosphorylates downstream MEK, which in turn bisphosphorylates ERK. ERK can then translocate to the nucleus, activating a variety of transcription factors and other nuclear substrates, as well as their cytoplasmic targets [42]. In mutant tumor cell lines harboring KRAS alleles, chemical inhibition of SOS1 resulted in a 50% reduction in p-ERK activity [34]. Our research results are largely consistent with previous findings and suggest that SOS1 promotes OC progression through ERK1/2. Notably, SOS1 inhibitors (BI-3406, NCT04924660) are being tested in Phase I trials for solid tumors, including OC [43]. This development provides a strong rationale for exploring combination therapies involving either CEBPB or ERK inhibitors as a promising therapeutic strategy for patients with PARPi-resistant OC.

While our study has elucidated a key mechanistic pathway through which CEBPB upregulates ERK1/2 activity via SOS1 to drive OC progression, we acknowledge certain limitations: The translational relevance of our findings would benefit from validation in patient-derived xenografts (PDXs) or primary tumor specimens, as these models more faithfully recapitulate human tumor biology [44–46].

Conclusion

In summary, our study demonstrates that CEBPB upregulates ERK1/2 activity and promotes the malignant progression of OC cells through SOS1. These findings provide a novel therapeutic target and a foundational theoretical basis for treating OC and overcoming associated drug resistance.

Acknowledgements We are grateful for the financial support received from the funders mentioned above.

Author contributions Jiahong Tan, Daoqi Wang, and Aiqing Tu contributed to the methodology, data acquisition, and analysis. Qin Xu, Li Zhuan, Xiaodie Wu, and Lin Zhao drafted the manuscript. Wei Dong, Jie Zhang, and Yun Feng conceived the study. All authors have read and agreed to this version of the manuscript. All authors contributed to the article and approved the submitted version.

Funding This work was supported by the National Natural Science Foundation of China (82203145), Yunnan Revitalization Talent Support Program (XDYC-QNRC-2023–0440), Joint Special Funds for the Department of Science and Technology of Yunnan Province-Kunming Medical University (202401AY070001-012), Basic Research Project of Yunnan Province (202301AT070041), Basic Research Project of Yunnan Province (202301AT070259), Yunnan Provincial Clinical Medical Research Center for Gynecological and Obstetrical Diseases (2023YJZX-FC08), National Key Clinical Specialty of Gynecology•First People's Hospital of Yunnan Province (2022FKZDZK-16), Yunnan Provincial Clinical Medical Center for Reproductive, Gynecological and Obstetrical Diseases (2022LCZXKF-SZ08), High-level Personnel Introduction Fund of the First People's Hospital of Yunnan Province (2022-KHRCBZ-B05), and Doctoral Research Fund Program of the First People's Hospital of Yunnan Province (KHBS-2022–026).

Data availability No datasets were generated or analysed during the current study.

Declarations

Conflict of interest The authors declare no competing interests.

References

1. Li S, Hongfu Z. 823TiP Fluzoparide combined with apatinib mesylate in the treatment of platinum resistant recurrent ovarian cancer: a single arm, single center, prospective clinical study. Ann Oncol. 2021. https://doi.org/10.1016/j.annonc.2021.08.1265.
2. Yousefi M, Dehghani S, Nosrati R, Ghanei M, Salmaninejad A, Rajaie S, Hasanzadeh M, Pasdar A. Current insights into the metastasis of epithelial ovarian cancer — hopes and hurdles. Cell Oncol (Dordr). 2020;43:515–38. https://doi.org/10.1007/s13402-020-00513-9.
3. Siegel RL, Giaquinto AN. Cancer statistics. CA A Cancer J Clin. 2024;74:12–49. https://doi.org/10.3322/caac.21820.

4. Sonkin D, Thomas A, Teicher BA. Cancer treatments: past, present, and future. Cancer Genet. 2024;286–287:18–24. https://doi.org/10.1016/j.cancergen.2024.06.002.
5. Huepenbecker SP, Sun CC, Fu S, Zhao H. Factors impacting the time to ovarian cancer diagnosis based on classic symptom presentation in the United States. Cancer. 2021;127:4151–60. https://doi.org/10.1002/cncr.33829.
6. Rao S, Smith DA. Past, present, and future of serum tumor markers in management of ovarian cancer: a guide for the radiologist. Radiographics. 2021;41:1839–56. https://doi.org/10.1148/rg.2021210005.
7. Pujade-Lauraine E, Ledermann JA, Selle F, Gebski V, Penson RT, Oza AM, Korach J, Huzarski T, Poveda A, Pignata S, Friedlander M, Colombo N, Harter P, Fujiwara K, Ray-Coquard I, Banerjee S, Liu J, Lowe ES, Bloomfield R, Pautier P. Olaparib tablets as maintenance therapy in patients with platinum-sensitive, relapsed ovarian cancer and a BRCA1/2 mutation (SOLO2/ENGOT-Ov21): a double-blind, randomised, placebo-controlled, phase 3 trial. Lancet Oncol. 2017;18:1274–84. https://doi.org/10.1016/s1470-2045(17)30469-2.
8. Zahnow CA. CCAAT/enhancer-binding protein beta: its role in breast cancer and associations with receptor tyrosine kinases. Expert Rev Mol Med. 2009;11: e12. https://doi.org/10.1017/s1462399409001033.
9. Li H, Yang F, Chai L, Zhang L, Li S, Xu Z, Kong L. CCAAT/enhancer binding protein β-mediated mmp3 upregulation promotes esophageal squamous cell cancer invasion in vitro and is associated with metastasis in human patients. Genet Test Mol Biomarkers. 2019;23:304–9. https://doi.org/10.1089/gtmb.2018.0291.
10. Ji Hae L, Jee Young S, Eun Kyung C, Hye-Jung Y, Bo K, Eun Kyung H, Byung-Kiu P, Yong-Nyun K, Seung Bae R, Kyungsil Y. C/EBPβ is a transcriptional regulator of Wee1 at the G2/M phase of the cell cycle. Cells. 2019. https://doi.org/10.3390/cells8020145.
11. Matherne MG, Phillips ES, Embrey SJ, Burke CM, Machado HL. Emerging functions of C/EBPβ in breast cancer. Front Oncol. 2023;13:1111522. https://doi.org/10.3389/fonc.2023.1111522.
12. Yang S, Wang J, Cheng R, Pang B, Sun P. LINC00035 transcriptional regulation of SLC16A3 via CEBPB affects glycolysis and cell apoptosis in ovarian cancer. Evid-Based Complement Altern Med. 2021;2021:5802082. https://doi.org/10.1155/2021/5802082.
13 Wu YH, Chang TH, Huang YF, Chen CC, Chou CY. COL11A1 confers chemoresistance on ovarian cancer cells through the activation of Akt/c/EBPβ pathway and PDK1 stabilization. Oncotarget. 2015;6:23748–63. https://doi.org/10.18632/oncotarget.4250.
14. Lord CJ, Ashworth A. PARP inhibitors: synthetic lethality in the clinic. Science. 2017;355:1152–8. https://doi.org/10.1126/science.aam7344.
15. Tan J, Zheng X, Li M. C/EBPβ promotes poly(ADP-ribose) polymerase inhibitor resistance by enhancing homologous recombination repair in high-grade serous ovarian cancer. Oncogene. 2021;40:3845–58. https://doi.org/10.1038/s41388-021-01788-4.
16. Liu D, Zhang XX, Li MC, Cao CH, Wan DY, Xi BX, Tan JH, Wang J, Yang ZY, Feng XX, Ye F, Chen G, Wu P, Xi L, Wang H, Zhou JF, Feng ZH, Ma D, Gao QL. C/EBPβ enhances platinum resistance of ovarian cancer cells by reprogramming H3K79 methylation. Nat Commun. 2018;9:1739. https://doi.org/10.1038/s41467-018-03590-5.
17. Schlessinger J. How receptor tyrosine kinases activate Ras. Trends Biochem Sci. 1993;18:273–5. https://doi.org/10.1016/0968-0004(93)90031-h.
18. Zarich N, Oliva JL, Martínez N, Jorge R, Ballester A, Gutiérrez-Eisman S, García-Vargas S, Rojas JM. Grb2 is a negative modulator of the intrinsic Ras-GEF activity of hSos1. Mol Biol Cell. 2006;17:3591–7. https://doi.org/10.1091/mbc.e05-12-1104.
19. Jeng HH, Taylor LJ, Bar-Sagi D. Sos-mediated cross-activation of wild-type Ras by oncogenic Ras is essential for tumorigenesis. Nat Commun. 2012;3:1168. https://doi.org/10.1038/ncomms2173.
20. Nakajima T, Kinoshita S, Sasagawa T, Sasaki K, Naruto M, Kishimoto T, Akira S. Phosphorylation at threonine-235 by a ras-dependent mitogen-activated protein kinase cascade is essential for transcription factor NF-IL6. Proc Natl Acad Sci USA. 1993;90:2207–11. https://doi.org/10.1073/pnas.90.6.2207.
21. Zhu S, Yoon K, Sterneck E, Johnson PF, Smart RC. CCAAT/enhancer binding protein-beta is a mediator of keratinocyte survival and skin tumorigenesis involving oncogenic Ras signaling. Proc Natl Acad Sci USA. 2002;99:207–12. https://doi.org/10.1073/pnas.012437299.
22. Wegner M, Cao Z, Rosenfeld MG. Calcium-regulated phosphorylation within the leucine zipper of C/EBP beta. Science. 1992;256:370–3. https://doi.org/10.1126/science.256.5055.370.
23. Giltiay NV, Karakashian AA, Alimov AP, Ligthle S, Nikolova-Karakashian MN. Ceramide- and ERK-dependent pathway for the activation of CCAAT/enhancer binding protein by interleukin-1beta in hepatocytes. J Lipid Res. 2005;46:2497–505. https://doi.org/10.1194/jlr.M500337-JLR200.
24. Peng C, Zhong F, Ling O, Yuanjing Z, Shuyi S, Hengrui L, Weichun Z, Gin Gin G, Guimin Z, Meicun Y. Syzygium aromaticum enhances innate immunity by triggering macrophage M1 polarization and alleviates Helicobacter pylori-induced inflammation. J Funct Foods. 2023. https://doi.org/10.1016/j.jff.2023.105626.
25. Ou L, Hao Y, Liu H, Zhu Z, Li Q, Chen Q, Wei R, Feng Z, Zhang G, Yao M. Chebulinic acid isolated from aqueous extracts of *Terminalia chebula* Retz inhibits *Helicobacter pylori* infection by potential binding to Cag A protein and regulating adhesion. Front Microbiol. 2024;15:1416794. https://doi.org/10.3389/fmicb.2024.1416794.
26. Liu H, Dilger JP, Lin J. Effects of local anesthetics on cancer cells. Pharmacol Ther. 2020;212:107558. https://doi.org/10.1016/j.pharmthera.2020.107558.
27. Zhong L, Yin R, Song L. Resistance to PARP inhibitors after first-line platinum-based chemotherapy in a patient with advanced ovarian cancer with a pathogenic somatic BRCA1 mutation. Pharmacogenom Personal Med. 2023;16:195–200. https://doi.org/10.2147/pgpm.s397827.
28. Ledermann JA, Pujade-Lauraine E. Olaparib as maintenance treatment for patients with platinum-sensitive relapsed ovarian cancer. Ther Adv Med Oncol. 2019;11:1758835919849753. https://doi.org/10.1177/1758835919849753.
29. McLachlan J, George A, Banerjee S. The current status of PARP inhibitors in ovarian cancer. Tumori. 2016;102:433–40. https://doi.org/10.5301/tj.5000558.
30. Cook SA, Tinker AV. PARP inhibitors and the evolving landscape of ovarian cancer management: a review. BioDrugs: Clin Immunother Biopharm Gene Ther. 2019;33:255–73. https://doi.org/10.1007/s40259-019-00347-4.
31. Konstantinopoulos PA, Ceccaldi R, Shapiro GI, D'Andrea AD. Homologous recombination deficiency: exploiting the fundamental vulnerability of ovarian cancer. Cancer Discov. 2015;5:1137–54. https://doi.org/10.1158/2159-8290.cd-15-0714.
32. Zhu H, Wei M, Xu J, Hua J, Liang C, Meng Q, Zhang Y, Liu J, Zhang B, Yu X, Shi S. PARP inhibitors in pancreatic cancer: molecular mechanisms and clinical applications. Mol Cancer. 2020;19:49. https://doi.org/10.1186/s12943-020-01167-9.
33. Basu SK, Gonit M, Salotti J, Chen J, Bhat A, Gorospe M, Viollet B. A RAS-CaMKKβ-AMPKα2 pathway promotes senescence by licensing post-translational activation of C/EBPβ through a novel

3'UTR mechanism. Oncogene. 2018;37:3528–48. https://doi.org/10.1038/s41388-018-0190-7.
34. Hillig RC, Sautier B, Schroeder J, Moosmayer D, Hilpmann A, Stegmann CM, Werbeck ND, Briem H, Boemer U, Weiske J, Badock V, Mastouri J, Petersen K, Siemeister G, Kahmann JD, Wegener D, Böhnke N, Eis K, Graham K, Wortmann L, von Nussbaum F, Bader B. Discovery of potent SOS1 inhibitors that block RAS activation via disruption of the RAS-SOS1 interaction. Proc Natl Acad Sci USA. 2019;116:2551–60. https://doi.org/10.1073/pnas.1812963116.
35. Winter JJ, Anderson M, Blades K, Brassington C, Breeze AL, Chresta C, Embrey K, Fairley G, Faulder P, Finlay MR, Kettle JG, Nowak T, Overman R, Patel SJ, Perkins P, Spadola L, Tart J, Tucker JA, Wrigley G. Small molecule binding sites on the Ras:SOS complex can be exploited for inhibition of Ras activation. J Med Chem. 2015;58:2265–74. https://doi.org/10.1021/jm501660t.
36. Howes JE, Akan DT, Burns MC, Rossanese OW, Waterson AG, Fesik SW. Small molecule-mediated activation of RAS elicits biphasic modulation of Phospho-ERK levels that are regulated through negative feedback on SOS1. Mol Cancer Ther. 2018;17:1051–60. https://doi.org/10.1158/1535-7163.mct-17-0666.
37. Diehl JN, Hibshman PS, Ozkan-Dagliyan I, Goodwin CM, Howard SV, Cox AD, Der CJ. Targeting the ERK mitogen-activated protein kinase cascade for the treatment of KRAS-mutant pancreatic cancer. Adv Cancer Res. 2022;153:101–30. https://doi.org/10.1016/bs.acr.2021.07.008.
38. Wortzel I, Seger R. The ERK cascade: distinct functions within various subcellular organelles. Genes Cancer. 2011;2:195–209. https://doi.org/10.1177/1947601911407328.
39. Zhang W, Liu HT. MAPK signal pathways in the regulation of cell proliferation in mammalian cells. Cell Res. 2002;12:9–18. https://doi.org/10.1038/sj.cr.7290105.
40. Peng M, Fan S, Li J, Zhou X, Liao Q, Tang F, Liu W. Programmed death-ligand 1 signaling and expression are reversible by lycopene via PI3K/AKT and Raf/MEK/ERK pathways in tongue squamous cell carcinoma. Genes Nutr. 2022;17:3. https://doi.org/10.1186/s12263-022-00705-y.
41. Wan W, Xiao W, Pan W, Chen L, Liu Z, Xu J. Isoprenylcysteine carboxyl methyltransferase is critical for glioblastoma growth and survival by activating Ras/Raf/Mek/Erk. Cancer Chemother Pharmacol. 2022;89:401–11. https://doi.org/10.1007/s00280-022-04401-x.
42. Macdonald SG, Crews CM, Wu L, Driller J, Clark R, Erikson RL, McCormick F. Reconstitution of the Raf-1-MEK-ERK signal transduction pathway in vitro. Mol Cell Biol. 1993;13:6615–20. https://doi.org/10.1128/mcb.13.11.6615-6620.1993.
43. Hofmann MH, Gmachl M, Ramharter J, Savarese F, Gerlach D. BI-3406, a POTENT and selective SOS1-KRAS interaction inhibitor Is Effective in KRAS-Driven Cancers through Combined MEK Inhibition. Cancer Discov. 2021;11:142–57. https://doi.org/10.1158/2159-8290.cd-20-0142.
44. Ru L, Yujie H, Hengrui L, James PD, Lin J. Abstract 2162: Comparing volatile and intravenous anesthetics in a mouse model of breast cancer metastasis. Can Res. 2018. https://doi.org/10.1158/1538-7445.am2018-2162.
45. Zi-Ran K, Shanshan J, Ji-Xuan H, Yaqi G, Yile X, Jinxian C, Qiang L, Jun Y, Xin Z, Jie H, Haoyan C, Yingxuan C, Huimin C, Jing-Yuan F. Deficiency of BCAT2-mediated branched-chain amino acid catabolism promotes colorectal cancer development. Biochimica et Biophysica Acta (BBA) — Molecular Basis of Disease. 2024. https://doi.org/10.1016/j.bbadis.2023.166941.
46. So Jeong L, SeongHo J, Sinyoung C, Chang Min K, Jung Ki Y, Seung-Hun O, Jong Hyup K, Young Y, JinKyeoung K. hsa-miR-CHA2, a novel microRNA, exhibits anticancer effects by suppressing cyclin E1 in human non-small cell lung cancer cells. Biochimica et Biophysica Acta (BBA) — Molecular Basis of Disease. 2024. https://doi.org/10.1016/j.bbadis.2024.167250.